IEEE Access
Multidisciplinary ⋮ Rapid Review ⋮ Open Access Journal

Received November 17, 2020, accepted November 29, 2020, date of publication December 3, 2020,
date of current version December 11, 2020.

Digital Object Identifier 10.1109/ACCESS.2020.3042343

System Identification Method Based on a Disturbance Observer Using Symmetric Reference Trajectories in PMLSM-Based Motion Systems

KWANGHYUN CHO[1], (Member, IEEE), AND KANGHYUN NAM[2], (Member, IEEE)
[1]Manufacturing Technology Center, Samsung Electronics Company Ltd., Hwaseong 443-742, South Korea
[2]School of Mechanical Engineering, Yeungnam University, Gyeongsan 712-749, South Korea

Corresponding author: Kanghyun Nam (khnam@yu.ac.kr)

This work was supported by the Korea Institute for Advancement of Technology (KIAT) Grant funded by the Korean Government (MOTIE) (HRD Program for Industrial Innovation) under Grant P0008473.

ABSTRACT This study is concerned with the problem of system identification for permanent magnet linear synchronous motor(PMLSM) based motion systems with disturbances such as parametric uncertainty, friction force, and force ripple. In order to identify the disturbances, a novel system identification method is proposed. The main idea of the proposed scheme is to separate and identify each element from a lumped disturbance by using even and odd characteristics of the state-dependent disturbances. The lumped disturbance is estimated by a linear disturbance observer(DOB), that includes the parametric errors, the friction force, and force ripple. To facilitate the decomposition of the lumped disturbance, the symmetric reference position trajectories are utilized, which make it useful to keep the even and odd characteristics of each element. The even and odd elements separated from the lumped disturbance by the decomposition method are represented as the force ripple multiplied by the mass error and the friction force multiplied by the viscous friction coefficient error, respectively. By comparing with experimental results based on different reference velocities and acceleration trajectories, the parametric errors are identified first, and then, nonlinear disturbances such as the force ripple and friction forces are identified by curve-fitting methods using the experimental data. The validity of the proposed scheme is illustrated by experimental tests. The effectiveness of the identified system elements is also verified by comparison with the position tracking performances of comparative studies.

INDEX TERMS System identification, symmetric reference trajectories, disturbance observer, permanent magnet linear synchronous motor, motion control.

I. INTRODUCTION

Precision motion control has received significant attention in modern control systems as an increasing number of mechanical devices such as semi-conductor fabrication equipment and liquid crystal display (LCD) panel transportation systems [1]–[4] require high-speed/high-accuracy position tracking performances. Due to their high force densities and high efficiencies, PMLSM-based motion systems are utilized widely for these applications. However, they have some difficulties in achieving high-precision position and speed control [5], [6]. Since the permanent magnet linear synchronous motor (PMLSM) contains the iron cores of the mover, it is directly affected by the force ripple including the detent force that occurs due to the attraction between the iron-cores of mover and permanent magnets. It is a position-dependent disturbance having a fundamental period similar to the pole pitch of permanent magnets. The friction force is also an obstacle to achieve high precision control. In the case of PLMSM-based motion systems using ball bearing guides, the motion accuracy and resolution may be limited due to guide friction [7]. The friction force has heavy nonlinearities at low velocity motions depending on the position as well as the velocity.

Numerous identification methods for the friction force and force ripple have already been proposed, but most of the

The associate editor coordinating the review of this manuscript and approving it for publication was Jianyong Yao.

existing methods for identifying these disturbances assume that the friction force and force ripple are decoupled by the structural characteristics of the motor, and are based on conservative assumptions. A compact model of the force generation that includes the effect of the ripple disturbance has been proposed [8] and [9], where experimental tests under very low constant-velocity motions were performed to obtain only the force ripple itself. However, an additional moving table is required to implement these tests. The identified force ripple may have the effect of the nonlinearity of the friction force due to experimental tests under very low velocity motions. In the studies [10] and [11], the force ripple was identified by measuring the control input signal at different load forces and position of the mover. However, these experimental tests require additional experimental setup such as force sensors, screw cylinder for manual position adjustment, a frictionless air bearing support, and moving carriage with pulleys and weights.

The friction force model based identification methods such as the generalized Maxwell-slip (GMS) model, variable natural length spring (VNLS) model, and rheology-based model have been also proposed [12]–[14]. The parameters of the proposed models are estimated by certain estimation methods. Since these models contain various parameters to be identified, it is difficult to guarantee that all the estimated parameters will converge to their actual values. On the contrary, the data-driven identification method is based on the measured friction data, which requires no mathematical models [15]. Instead of the approximated models, the friction data table is stored in memory. From the friction table, the friction force is reproduced by the corresponding displacement. However, this scheme requires a variety of experimental tests to describe the physical characteristics of the rolling friction. Therefore, developing an accurate friction table is time-consuming, and the table must be also revised depending on the operating conditions of the PMLSM-based motion systems. A simple sinusoidal model was used to represent the characteristics of the force ripple, whose parameters were estimated by adaptive control schemes [16], [17]. However, the force ripple may have different magnitudes depending on the position since each permanent magnet on the long stroke cannot have the same magnetic characteristics perfectly unlike rotary motors. Therefore, this cannot describe the actual force ripple precisely. Moreover, it is very sensitive to the model uncertainties compared to the rotary motor since the mechanical transmissions such as the belt and pulley, rack and pinion, and lead and ball-screw are eliminated here.

In this study, a system identification method is proposed to identify the parametric errors, friction force, and force ripple in PMLSM-based motion systems. The proposed scheme does not use any conservative assumptions and additional hardware such as actuators and sensors. The main idea of the proposed scheme is to separate and identify each element from a lumped disturbance by using even and odd characteristics of the state-dependent disturbances. Therefore, each disturbance can be identified more precisely when it is compared with other methods that have no initial conditions for each disturbance. The lumped disturbance is estimated by a linear disturbance observer(DOB), that includes the parametric errors, friction force, and force ripple. To facilitate the decomposition of the lumped disturbance, the symmetric reference position trajectories are utilized, which make it useful to keep the even and odd characteristics of each element. By comparing with experimental results based on different reference velocities and acceleration trajectories, the parametric errors are identified first, and then, nonlinear disturbances such as the force ripple and friction forces are identified by curve-fitting methods using the experimental data. The validity of the proposed scheme is illustrated by experimental tests. The effectiveness of the identified system elements is also verified by comparison with the position tracking performances of comparative studies.

This paper is organized as follows. In section II, the dynamic model and controller of the PMLSM-based motion systems are introduced. In section III, a system identification method is illustrated. Experimental validations are given stated in section IV. Finally, section V provides some concluding remarks.

II. THE PMLSM-BASED MOTION SYSTEMS

In this section, mathematical models of the PMLSM-based motion system and its controller are illustrated, which can minimize the position tracking error and to estimate a lumped disturbance.

A. MATHEMATICAL MODEL

From the force balance equation, the mechanical dynamics of the PLMSM-based motion system is presented as follows:

$$M\ddot{x}(t) = -B\dot{x}(t) + u(t) - F_{fric}(x, \dot{x}) - F_{rip}(x) - F_{ex}(t) \tag{1}$$

where $x(t)$ is position, M the mass, B the viscous friction coefficient, $u(t)$ control input, $F_{fric}(x, \dot{x})$ the friction force, $F_{rip}(x)$ the force ripple, and $F_{ex}(t)$ the external disturbance. Since the friction force and force ripple are dominant disturbances which can degrade the position tracking performance, the external disturbance can be ignored for simplicity. (i.e., $F_{ex}(t) = 0$) The electrical dynamics is also ignored because the electrical dynamics is fast enough comparing with the frequency bandwidth of the interest [18].

B. CONTROLLER DESIGN

Generally, the model parameters can be obtained by a general system identification method such as the sine-sweep test. Considering the known model parameters, (1) can be represented as follows:

$$M_n\ddot{x}(t) = -B_n\dot{x}(t) + u(t) + d(t), \tag{2}$$

where M_n and B_n are the known nominal values of the mass and viscous friction coefficient, respectively. In (2), the lumped disturbance $d(t)$ consists of the parametric errors, the

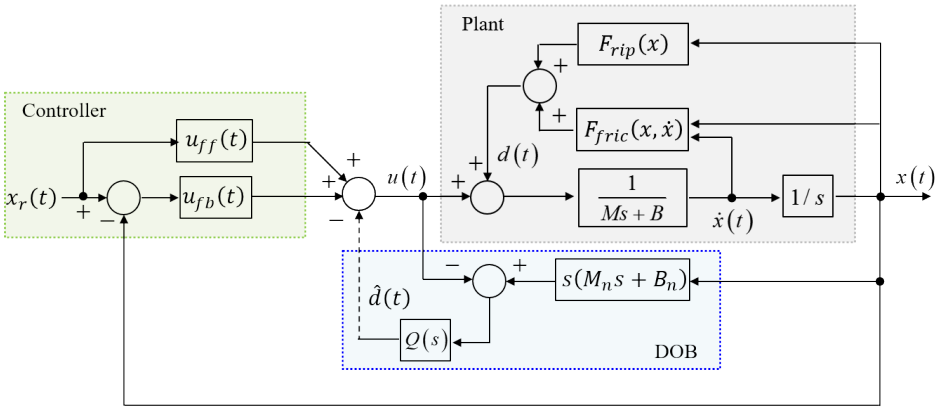

FIGURE 1. The proposed control scheme based on disturbance observer.

friction force, and the force ripple, as which can be written as follows:

$$d(t) = -\Delta M\ddot{x}(t) - \Delta B\dot{x}(t) - F_{fric}(x,\dot{x}) - F_{rip}(x), \quad (3)$$

where $\Delta M = M - M_n$ and $\Delta B = B - B_n$ are the parametric errors.

The proposed controller is shown in Fig. 1. Based on the nominal model given by (2), a position tracking controller that has following control inputs is designed to track the reference trajectories with tracking errors as small as possible:

$$u(t) = u_{fb}(t) + u_{ff}(t) - \hat{d}(t). \quad (4)$$

Here, $u_{fb}(t)$ and $u_{ff}(t)$ are the feedback and feedforward control inputs, respectively. $\hat{d}(t)$ is the lumped disturbance estimated by a linear disturbance observer(DOB). It has been utilized for simplicity although there exist advanced disturbance observers [19]–[21].

Then, each control input can be designed as follows:

$$u_{fb}(t) = K_D\dot{e}_x(t) + K_P e_x(t) + K_I\int_0^t e_x(\tau)d\tau, \quad (5)$$

$$u_{ff}(t) = M_n\ddot{x}_r(t) + B_n\dot{x}_r(t), \quad (6)$$

$$\hat{d}(t) = Q(t) * \left[M_n\ddot{x}(t) + B_n\dot{x} - u(t)\right]. \quad (7)$$

where $e_x(t) = x_r(t) - x(t)$ is the position tracking error, $x_r(t)$ the reference position trajectory, K_P, K_I, and K_D the PID gains. The overall system can be stable since all desired poles are designed to be located on the left-half plane by selecting the PID gains [22].

In (7), the velocity and acceleration information are obtained by the derivative of the position. Since the noise effect is amplified due to the derivative of the position, the ESO-based methods can be helpful to obtain the velocity and acceleration information [23], [24]. In this study, the Q-filter(low pass filter), $Q(t)$, is utilized to attenuate the amplified noise effect. It guarantees that the actual plant behaves as the nominal model since the low-frequency components of the disturbance are estimated and attenuated by DOB without the noise effect. More detailed DOB design methodologies are presented in numerous studies [25], [26].

Using (2) and (3), the estimated lumped disturbances can be rewritten as follows:

$$\hat{d}(t) = Q(t) * \left[-\Delta M\ddot{x}(t) - \Delta B\dot{x} - F_{fric}(x,\dot{x}) - F_{rip}(x)\right]. \quad (8)$$

Since the cut-off frequency of the Q-filter is limited due to the existence of the noise or unmodeled dynamics, the estimated disturbance may have phase lag, and the distortion of magnitude in the frequency range may be beyond the cut-off frequency of the Q-filter. However, these weaknesses of the estimated disturbance are compensated by the proposed scheme easily.

III. A NOVEL SYSTEM IDENTIFICATION METHOD

In this section, a system identification in PMLSM-based motion systems is illustrated, that uses even and odd characteristics of the state-dependent characteristics of system elements.

A. SELECTION OF REFERENCE TRAJECTORY

The parametric errors as well as the friction force and force ripple are coupled with the states such as the position, velocity and acceleration as shown in (3). The main idea of the proposed system identification method is to separate and identify each element coupled with states from the lumped disturbance by using the even and odd characteristics of the state-dependent disturbances.

To ensure that each element in (3) cantains even and odd characteristics, the proposed scheme utilizes symmetric position reference trajectories. In this case, the generated position, velocity, and acceleration states can be described as even functions, and that of the velocity state can be described as odd functions assuming that a high-accuracy position tracking performance is guaranteed by the designed controller. Then, the mass error multiplied by the acceleration and the force ripple can be considered as even elements, while the viscous friction coefficient error multiplied by velocity and the friction force as odd elements. Therefore, all the

state-dependent elements now have either even or odd characteristics.

There are several types of symmetric reference trajectories such as the sinusoidal, trapezoidal and bell-type. In the proposed scheme, the bell-type position reference trajectory is used, because the following properties are guaranteed to separate and identify each element from the lumped disturbance:

- The reference position/velocity/acceleration trajectories have the characteristics of even/odd/even functions, and these are smooth enough to achieve high-accuracy position tracking performances.
- The reference position trajectory is long enough to describe the force ripple.
- The reference velocity trajectory has a variety of operating velocity points to describe the characteristics of the friction force with the hysteresis effects and the viscous friction simultaneously.
- The reference acceleration trajectory is smooth enough to present the effect of mass error.

The mathematical representation of the used reference trajectory is written as follows:

$$x_r(t)=\begin{cases} -(\dot{x}_r)_{max}\dfrac{8}{15}\left(\dfrac{T_r}{2}\right)^2\left\{15\left(\dfrac{\tau}{T_r/2}\right)^4 \right. \\ \left. -6\left(\dfrac{\tau}{T_r/2}\right)^5-10\left(\dfrac{\tau}{T_r/2}\right)^3\right\} \\ \qquad\qquad \text{for} \quad 0\le\tau<T_r/2, \\ -(\dot{x}_r)_{max}\dfrac{8}{15}\left(\dfrac{T_r}{2}\right)^2\left\{15\left(\dfrac{\tau-T_r}{T_r/2}\right)^4 \right. \\ \left. -6\left(\dfrac{\tau-T_r}{T_r/2}\right)^5-10\left(\dfrac{\tau-T_r}{T_r/2}\right)^3\right\} \\ \qquad\qquad \text{for} \quad T_r/2\le\tau<T_r, \end{cases} \tag{9}$$

where $(\dot{x}_r)_{max}$ is the maximum value of the reference velocity trajectory, T_r the time period of the reference trajectories, $\tau = t-(T_r\cdot m)$ the virtual time variable, t the time, and $m = 0, 1, 2, \ldots$ the iteration number. Equation (9) shows the trajectory modified for back-and-forth motion of the trajectory used in the study [16].

B. DECOMPOSITION METHOD

Based on the symmetric reference trajectory in (9), the position tracking control is performed to estimate the lumped disturbance by the disturbance observer (7). The estimated lumped disturbance (8) is separated into the even and odd parts by the proposed decomposition method, which is a preprocessing step to identify each element in (8). When the sample time is given as T_{sm} and the estimated lumped disturbance for one time period ($0 \le t \le T_r$) is saved in memory, the total number of samples of the saved disturbance becomes equal to $N = T_r/T_{sm}+1$. Using the sample index k, the estimated lumped disturbance can be decomposed into even and odd parts for a half time period ($0 \le t \le T_r/2$) by the following equation:

$$[\hat{d}(k)]_{even} = \frac{1}{2}\Big[\hat{d}(k)+\hat{d}(N-k+1)\Big], \tag{10}$$

$$[\hat{d}(k)]_{odd} = \frac{1}{2}\Big[\hat{d}(k)-\hat{d}(N-k+1)\Big], \tag{11}$$

where $\hat{d}(N-k+1)$ indicates the flipped signal of $\hat{d}(k)$ over the y-axis at $k=(N-1)/2+1$ and $1\le k\le(N-1)/2+1$.

Assuming that $x(k) = x(N-k+1)$, $\dot{x}(k) = -\dot{x}(N-k+1)$ and $\ddot{x}(k) = \ddot{x}(N-k+1)$ due to the even and odd characteristics of the states, the even and odd parts can be represented as follows:

$$\begin{aligned}[\hat{d}(k)]_{even} = &-\Delta\hat{M}\ddot{x}(k)-[\hat{F}_{rip}(x(k))]_{even} \\ &-[\hat{F}_{fric}\big(x(k),\dot{x}(k)\big)]_{even},\end{aligned} \tag{12}$$

$$[\hat{d}(k)]_{odd} = -\Delta\hat{B}\dot{x}(k)-[\hat{F}_{fric}\big(x(k),\dot{x}(k)\big)]_{odd} \tag{13}$$

In (12), the even part is presented as the estimation of the sum of the mass error multiplied by the acceleration and the even components of the force ripple and the friction force. Here, the mass error multiplied by the acceleration and the force ripple are dominant components since $x(k)$ and $\ddot{x}(k)$ are described as the even functions. The even component of the friction force $\big[\hat{F}_{fric}\big(x(k),\dot{x}(k)\big)\big]_{even}$ arises due to the existence of the hysteresis effect of the friction force. This term can be negligible when the mover of PMLSM-based motion systems moves. In the case that there exists the hysteresis effect of the friction force exists, the even component of the friction force should be separated from the estimated even disturbance to identify the force ripple more precisely. Since the hysteresis effect varies more rapidly compared to the mass error multiplied by the acceleration and the force ripple, it can be separated easily from (12). Here, the phase lag problem induced by the Q-filter in the estimated lumped disturbance is compensated by (12) because the phase lag problem of $\hat{d}(k)$ can be nullified by the phase lead effect induced by $\hat{d}(N-k+1)$. This is considered as an advantage of the proposed decomposition method.

The odd part in (13) represents the estimation of the sum of the viscous friction coefficient error multiplied by the velocity and the odd components of the friction force and force ripple. Here, the viscous friction coefficient error and the friction force are dominant components in $[\hat{d}(k)]_{odd}$ because $\dot{x}(k)$ is described as an odd function.

C. PARAMETRIC ERROR IDENTIFICATION

Since the hysteresis effect of the friction force in the even disturbance can be negligible due to the movement of the mover of PMLSM-based motion systems, (12) is approximated as follows:

$$[\hat{d}(k)]^m_{even} = -\Delta\hat{M}\ddot{x}(k)-[\hat{F}_{rip}(x(k))]_{even}. \tag{14}$$

The mass error ΔM is constant and the force ripple is a function of its position. The decomposition of the mass error and the force ripple from (14) can be achieved by comparison

of the experimental results that have different reference acceleration trajectories but same reference position trajectories.

For example, we assume that two experimental tests, where a PMLSM-based motion system tracks to the same reference position but different reference acceleration trajectories in the sample-domain (i.e., $x_{1r}(k) = x_{2r}(k)$ and $\ddot{x}_{1r}(k) = (1/n)\cdot\ddot{x}_{2r}(k)$, where n is a non-zero real number) are carried out. These trajectories can be implemented using different sampling times though two reference position trajectories are different in the time-domain (i.e., $x_{1r}(t) \neq x_{2r}(t)$ and $\ddot{x}_{1r}(t) \neq \ddot{x}_{2r}(t)$, where t is the time variable). Assuming that a superior tracking performance is guaranteed (i.e., $x_1(k) = x_{1r}(k)$ and $x_2(k) = x_{2r}(k)$), the even part can be written as follows:

$$[\hat{d}_1(k)]^m_{even} = -\Delta\hat{M}\ddot{x}_1(k) - [\hat{F}_{rip}(x_1(k))]_{even}, \quad (15)$$

$$[\hat{d}_2(k)]^m_{even} = -n\cdot\Delta\hat{M}\ddot{x}_1(k) - [\hat{F}_{rip}(x_2(k))]_{even}. \quad (16)$$

Since the induced force ripples are identical in two cases due to the same reference position trajectories (i.e., $[\hat{F}_{rip}(x_1(k))]_{even} = [\hat{F}_{rip}(x_2(k))]_{even}$ due to $x_1(k) = x_2(k)$ and $[F_{rip}(x_1(k))]_{even} = [F_{rip}(x_2(k))]_{even}$), the mass error can be calculated as follows:

$$\Delta\hat{M} = \frac{[\hat{d}_2(k)]^m_{even} - [\hat{d}_1(k)]^m_{even}}{\ddot{x}_2(k) - \ddot{x}_1(k)} \quad (17)$$

The viscous friction coefficient error $\Delta\hat{B}$ can be identified by comparing the slopes of the data distribution of the odd disturbances estimated by experimental tests where the PMLSM-based motion system tracks to different reference velocity trajectories.

D. FORCE RIPPLE IDENTIFICATION

After the parametric errors are identified, the force ripple and friction force are identified from the even and odd parts. When the even and odd parts are compensated by the identified parametric errors, (12) and (13) can be rewritten as follows:

$$\begin{aligned}[\hat{d}(k)]^c_{even} &= [\hat{d}(k)]_{even} + \Delta\hat{M}\ddot{x}(k)\\ &= -[\hat{F}_{rip}(x(k))]_{even} - \left[\hat{F}_{fric}\left(x(k),\dot{x}(k)\right)\right]_{even}, \quad (18)\\ [\hat{d}(k)]^c_{odd} &= [\hat{d}(k)]_{odd} + \Delta\hat{B}\dot{x}(k)\\ &= -\left[\hat{F}_{fric}\left(x(k),\dot{x}(k)\right)\right]_{odd} \quad (19)\end{aligned}$$

The even element of the friction force occurs due to the hysteresis effect of the friction force. Since this effect does not appear when nearly moving, the force ripple is directly estimated by (18) (i.e., $\left[\hat{F}_{fric}\left(x(k),\dot{x}(k)\right)\right]_{even} = 0$). When the hysteresis effect of the friction force exists, it should be separated from (18) to identify the force ripple more precisely (i.e., $\left[\hat{F}_{fric}\left(x(k),\dot{x}(k)\right)\right]_{even} \neq 0$). Since this effect appears rapidly close to zero velocity conditions and the force ripple cannot be varied suddenly within hundreds of micrometers, both elements can be separated easily. The estimated even part without the even element of the friction force becomes the estimated force ripple as given:

$$\hat{F}_{rip}(x(k)) = -[\hat{d}(k)]^c_{even} - \left[\hat{F}_{fric}\left(x(k),\dot{x}(k)\right)\right]_{even}. \quad (20)$$

E. FRICTION FORCE IDENTIFICATION

The friction force model can be determined by the existence of the even element of the friction force in (12), and then the total friction force model is identified by the combination of the even and odd elements of the friction force in (18) and (19). Since the friction force is based on the static friction force model at the steady state even though it shows the hysteresis effect, the static friction force model is identified priorly by the estimated odd part. Assuming that the odd element of the force ripple can be considered negligible to identify the friction force since its effect is mostly presented over a certain velocity where the friction force is only described as the Coulomb friction force only, the data distribution for identifying the static friction force is obtained by the estimated odd parts from the experimental results that have different reference velocity trajectories. From the data distribution, the parameters of the static friction model are determined by the curve-fitting method. The friction model used to describe the static friction force is written as follows:

$$g(\dot{x}(k)) = (f_c + (f_s - f_c))\cdot\exp(-|\dot{x}(k)/\dot{x}_s|^2)\cdot\mathrm{sgn}(\dot{x}(k)), \quad (21)$$

where f_c is the Coulomb friction force, f_s the static friction force, and $\dot{x}_s$ the Striebeck velocity. Here, the definition of $\mathrm{sgn}(\dot{x}(k))$ is as follows:

$$\mathrm{sgn}(\dot{x}(k)) = \begin{cases} -1 & \text{if } \dot{x}(k) < 0\\ 0 & \text{if } \dot{x}(k) = 0\\ 1 & \text{if } \dot{x}(k) > 0. \end{cases}$$

In this study, the parameter identification method that represents the sum of the errors between the data distribution and friction force model minimizing the cost function is utilized. The utilized cost function can be presented as follows:

$$\min_{\hat{\theta}_1,\hat{\theta}_2,\hat{\theta}_3} J = \sum_{k=1}^{N}\Big[-\left[\overline{d(\dot{x}(k))}\right]^c_{odd} - \left((\hat{\theta}_1 + (\hat{\theta}_2 - \hat{\theta}_1))\cdot\exp(-|\dot{x}(k)/\hat{\theta}_3|^2)\cdot\mathrm{sgn}(\dot{x}(k))\right)\Big]^2, \quad (22)$$

where

$$\left[\overline{d(\dot{x}(k))}\right]^c_{odd} = \left[[\hat{d}_1(k)]^c_{odd} \quad [\hat{d}_2(k)]^c_{odd} \quad \cdots \quad [\hat{d}_i(k)]^c_{odd}\right]. \quad (23)$$

Here, $\left[\overline{d(\dot{x}(k))}\right]^c_{odd}$ signifies the data distribution of the estimated odd disturbances along the velocity of the mover that is obtained by several experimental tests, and i is the number of the tests. $\hat{\theta}_1 \sim \hat{\theta}_3$ are the parameters to be identifed for describing the static friction force model, which is finally determined based on the identified parameters.

When the hysteresis effect of the friction force exists, the separated even element of the friction force is added to the

estimated odd part. The sum of the even and odd elements of the friction force is used to generate the data distribution of the friction force with the hysteresis effect. In this study, the LuGre friction model is utilized to describe the dynamic friction force that is the static friction force with hysteresis effect as follows:

$$\frac{dz(t)}{dt} = \dot{x}(t) - \rho_0 \frac{|\dot{x}(t)|}{g(\dot{x}(t))} z(t), \tag{24}$$

$$F_{fric}\big(x(t), \dot{x}(t)\big) = \rho_0 z(t) + \rho_1 \dot{z}(t), \tag{25}$$

where $z(t)$ is the internal friction state and $F_{fric}\big(x(t), \dot{x}(t)\big)$ is the predicted total friction force. The state $z(t)$ is interpreted as the average bristle deflection. The LuGre model reproduces spring-like behavior for small displacements, where the parameter ρ_0 is the stiffness and ρ_1 is the micro damping. More details regarding the LuGre friction model is given here [27].

The parameters of the LuGre friction model are obtained by the parameter identification method minimizing the cost function that is presented as the sum of the errors between the data distribution and friction force model in common with (22), and the utilized cost function is presented as follows:

$$\min_{\hat{\rho}_0, \hat{\rho}_1} J = \sum_{k=1}^{N} \Big[-\overline{F}_{fric}\big(x(k), \dot{x}(k)\big) - \big(\hat{\rho}_0 z(k) + \hat{\rho}_1 \cdot \dot{z}(k)\big) \Big]^2, \tag{26}$$

where

$$\overline{F}_{fric}\big(x(k), \dot{x}(k)\big) = \big[\hat{F}_{fric}\big(x_1(k), \dot{x}_1(k)\big) \cdots \hat{F}_{fric}\big(x_i(k), \dot{x}_i(k)\big)\big], \tag{27}$$

and

$$\hat{F}_{fric}\big(x_i(k), \dot{x}_i(k)\big) = [\hat{d}_i(k)]^c_{odd} - [\hat{F}_{fric}\big(x_i(k), \dot{x}_i(k)\big)]_{even}. \tag{28}$$

Here, $\overline{F}_{fric}\big(x(k), \dot{x}(k)\big)$ represents the data distribution of the sum of the estimated odd part and even element of the friction force along the velocity of the mover that is obtained by several experimental tests (i-times of experimental tests). The static friction model represented by (21) and (22) is utilized to describe the dynamic friction model given by (24) and (25). $\hat{\rho}_0$ and $\hat{\rho}_1$ are the parameters to be identified to describe the dynamic friction force model. Finally, the total friction force model is determined as $\hat{F}_{fric}\big(x(k), \dot{x}(k)\big)$ based on the identified parameters.

IV. EXPERIMENTAL VERIFICATION

In this section, the procedures of the proposed scheme are illustrated, and its effectiveness is verified by the position tracking controller based on the identified system.

TABLE 1. The specification of PMLSM-based motion system.

Parameters	$M[kg]$	$B[N/m/s^2]$	$Kf[N/A]$
values	8.7	80.7	32.9838

TABLE 2. Variables in the reference trajectories.

	T_r[sec]	$(\dot{x}_r)_{max}$[m/s]	T_s[sec]	Total samples
EXP1('v025')	8	0.025	0.0008	10001
EXP2('v050')	4	0.050	0.0004	10001
EXP3('v100')	2	0.100	0.0002	10001
EXP4('v200')	1	0.200	0.0001	10001

A. EXPERIMENTAL SETUP

The experimental setup is shown in Fig. 2. All experiments were carried out based on the prototype of the PMLSM-based motion system depicted in Fig. 3. The specification of PMLSM-based motion system is presented in Table 1. A PWM inverter having a 20 kHz switching frequency was utilized and controlled by a dSPACE DS1103 board. The position controller was designed by Matlab/Simulink and it was executed at 0.5 ms loop time. An optical linear encoder, which has a resolution of 0.5 μm, was utilized to measure the position of the PMLSM. The controller

B. SELECTION OF REFERENCE TRAJECTORY

The proposed scheme utilizes the bell-type reference position trajectory shown in (9). To facilitate to decomposition of the estimated lumped disturbance, four experimental tests containing the different parameters already presented in Table. 2 are carried out, and these reference trajectories are shown in Fig. 4. Fig. 4(a), 4(c), and 4(e) show the trajectories in the time-domain, while Fig. 4(b), 4(d) and 4(f) show the trajectories in the sample-domain. In these figures, it is seen that when the reference position trajectories in each experimental test are defined as $x_{1r}(t)$, $x_{2r}(t)$, $x_{3r}(t)$ and $x_{4r}(t)$, all the reference trajectories have following properties:

- $x_{1r}(t) \neq x_{2r}(t) \neq x_{3r}(t) \neq x_{4r}(t)$,
  but $x_{1r}(k) = x_{2r}(k) = x_{3r}(k) = x_{4r}(k)$,
- $\dot{x}_{1r}(t) \neq \dot{x}_{2r}(t) \neq \dot{x}_{3r}(t) \neq \dot{x}_{4r}(t)$,
  but $8{\cdot}\dot{x}_{1r}(k) = 4{\cdot}\dot{x}_{2r}(k) = 2{\cdot}\dot{x}_{3r}(k) = \dot{x}_{4r}(k)$,
- $\ddot{x}_{1r}(t) \neq \ddot{x}_{2r}(t) \neq \ddot{x}_{3r}(t) \neq \ddot{x}_{4r}(t)$,
  but $64{\cdot}\ddot{x}_{1r}(k) = 16{\cdot}\ddot{x}_{2r}(k) = 4{\cdot}\ddot{x}_{3r}(k) = \ddot{x}_{4r}(k)$,

where k is the sample index ($0 \leq k \leq N$, N is the total number of samples for one time period).

If superior position tracking performances in all the experimental tests are guaranteed under the reference trajectories based on these properties, the following advantages can be utilized for the proposed disturbance identification method:

- Since all the acceleration signals can be expressed as multiples of $\ddot{x}_{1r}(k)$ and the same force ripples are occurred, the use of (17) facilitates the identification of the mass error.
- The force ripples occurring in all the experimental tests become identical due to the same reference position trajectories.

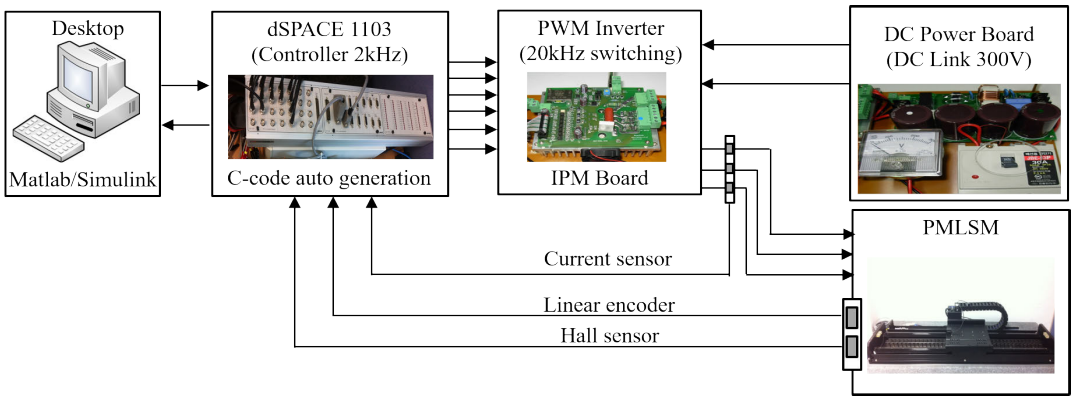

FIGURE 2. Experimental setup.

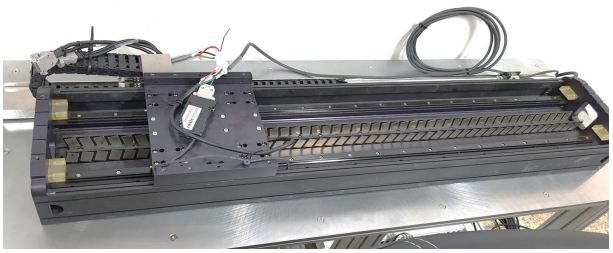

FIGURE 3. Experimental PMLSM-based motion system.

- Due to the variety of the operating velocity points, the characteristics of the friction force including the viscous friction coefficient error can be described.

C. DECOMPOSITION OF LUMPED DISTURBANCES

In the experimental tests, a simple 2-DOF feedback controller with DOB as shown in (4) was used to the track reference trajectories described in Fig. 4. The Q-filter having a cutoff frequency of 16Hz was utilized to include all the fundamental frequency of the force ripple varying along the velocity in the estimated lumped disturbance.

When the reference trajectories shown in Fig. 4 are applied, the disturbances estimated in all the experimental tests are shown in Fig. 5. In particular, the lumped disturbances estimated by (7) are shown in Fig. 5(a) and 5(b). Rearranging the estimated disturbances in the time domain as described in Fig. 5(a) to those in the sample domain as described in Fig. 5(b), it is seen that all the experimental results show similar patterns. Using (10) and (11), these lumped disturbances are decomposed into even and odd parts as shown in Fig. 5(c) and 5(d). When the even and odd parts in the time-domain are rearranged in the sample-domain as shown in Fig. 5(c) and 5(d), it is verified that the characteristics of the force ripple and the friction force are presented quite well.

D. IDENTIFICATION OF PARAMETRIC ERRORS

Fig. 6(a) shows that there exist little differences among the estimated even parts at a constant sample number. Especially,

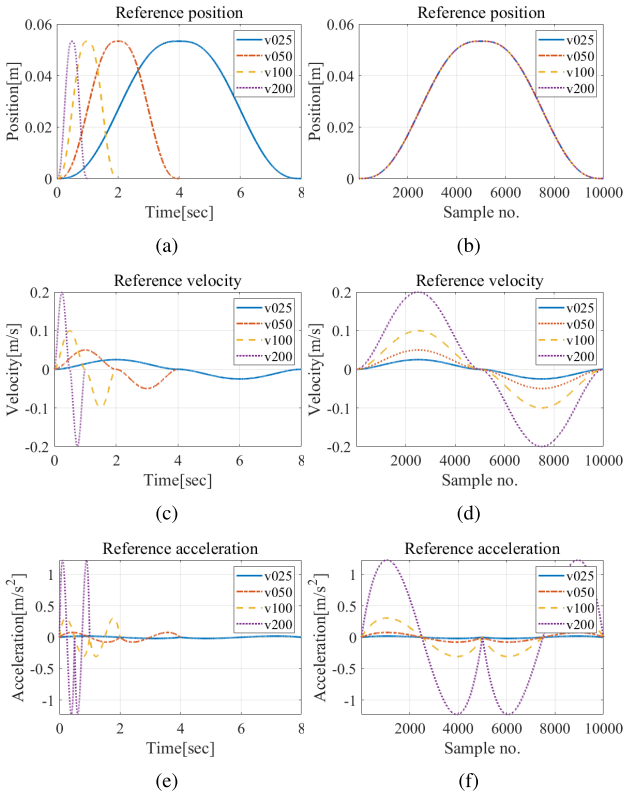

FIGURE 4. Reference trajectories: (a) Reference position trajectories in the time domain. (b) Reference position trajectories in the sample domain. (c) Reference velocity trajectories in the time domain. (d) Reference velocity trajectories in the sample domain. (e) Reference acceleration trajectories in the time domain. (f) Reference acceleration trajectories in the sample domain.

it is verified that the difference increases as the velocity and acceleration are increased. Since the components on the left and right-hand-sides are considered as $\left[\hat{F}_{fric}\left(x(k), \dot{x}(k)\right)\right]_{even}$ in (12) and the force ripples occurring in all the experiments are nearly identical, these differences shown in Fig. 6(a) can be considered as $-\Delta\hat{M}\ddot{x}(k)$. Therefore, the mass errors for the comparison among the experimental tests can be identified by (17), and it is identified as $\Delta M = -2.0kg$ as shown

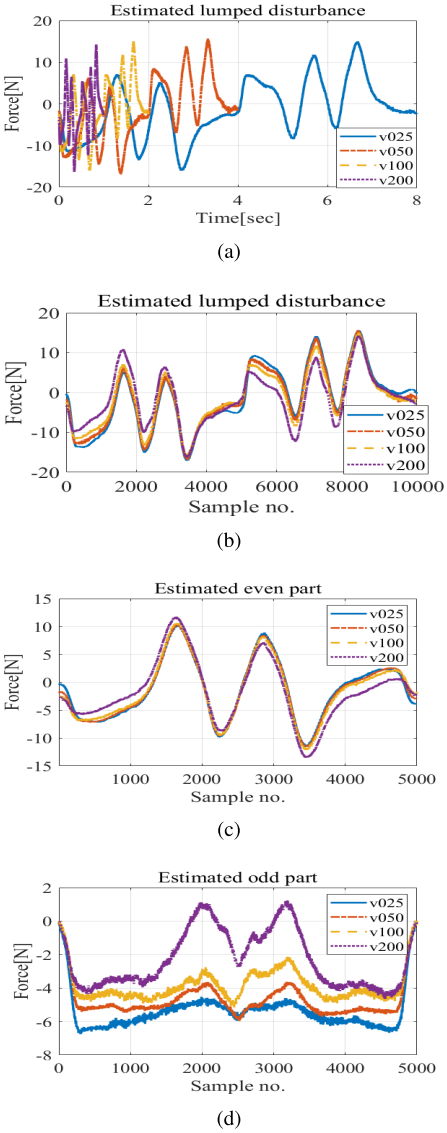

FIGURE 5. Estimated disturbances: (a) Estimated lumped disturbance in the time domain. (b) Estimated lumped disturbance in the sample domain. (c) Estimated even part in the sample domain. (d) Estimated odd part in the sample domain.

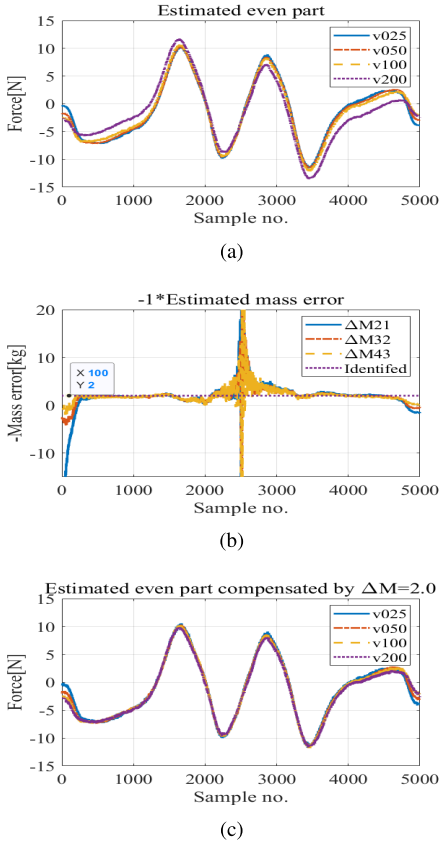

FIGURE 6. Even part: (a) Estimated even part in the sample domain. (b) Estimated mass error in the sample domain. (c) Estimated even part compensated by $\Delta M = -2.0kg$ in the sample domain.

in Fig. 6(b). ΔM should be selected as an average value of all experimental results. The tracking control performance in the acceleration region can be varied depending on the mass error because this parameter is used for the feedforward control input. To check the accuracy of the identified mass error, the even parts compensated for by the identified mass error in (18) are presented in Fig. 6(c). As shown in this figure, the differences among the even parts become smaller, and it is verified that the estimated mass error becomes nearly zero when (17) is applied to the even parts compensated by the mass error. Therefore, it can be verified that the accurate mass error is identified easily by the proposed method.

The viscous friction coefficient error $\Delta\hat{B}$ can be identified by calculating the slopes of the obtained odd parts. Unlike the estimated even parts, the odd parts of different experimental results have a lot of differences among them, especially at low velocities. However, since the slopes of the odd disturbances are similar, the viscous friction coefficient error can be identified easily. ΔB should be selected as a minimum slope of all experimental results to avoid the distortion of the odd disturbances induced by accelerated motion. The tracking control performance in the acceleration region can be varied depending on the viscous friction coefficient error because this parameter is used for the feedforward control input like the mass error ΔM. As shown in Fig. 7(a), it is verified that the viscous friction coefficient error is about $\Delta\hat{B} = -23N/m/s$ by calculating the slope of the disturbances. To check whether an accurate viscous friction coefficient error is identified, the odd parts compensated by the identified viscous friction coefficient error are presented in Fig. 7(b). As shown in this figure, it is verified that the slope of the odd parts becomes nearly zero. From these experimental results, it is verified that the parametric errors are identified easily by the proposed scheme.

E. IDENTIFICATION OF FORCE RIPPLE AND FRICTION FORCE

Based on the even and odd parts compensated by the parametric errors in (18) and (19), the force ripple and the friction

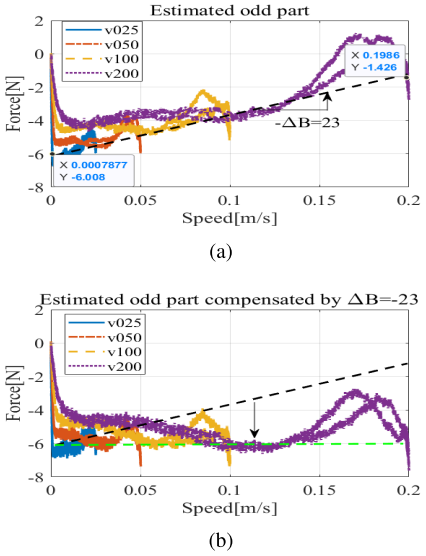

FIGURE 7. Odd part: (a) Estimated odd parts and the viscous friction coefficient error in the velocity domain. (b) Estimated odd part with $\Delta B = -23N/m/s$ in the velocity domain.

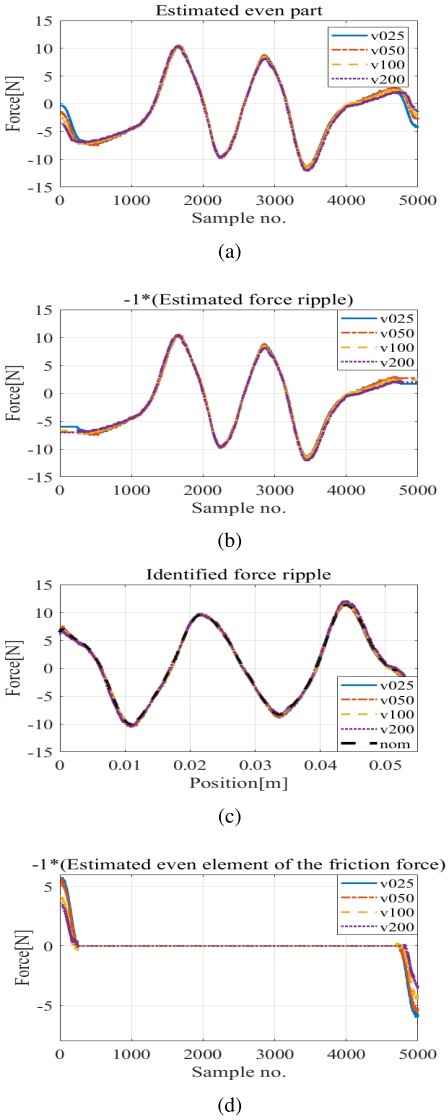

FIGURE 8. Identification of the force ripple and the even element of the friction force: (a) Even part in the sample domain. (b) Even part without the even components of the friction force in the sample domain. (c) Identified force ripples in the position domain. (d) Even element of the friction force in the sample domain.

force are identified. It is important that the even components of the friction force, that represent the hysteresis effect of the friction force, are separated from the estimated even parts to identify the force ripple and the friction force more precisely. The hysteresis effect of the friction force appears to be dominant near the zero velocity condition, and the force ripple that is a position-dependent disturbance cannot vary rapidly within hundreds of micrometers ($60um$). Thus, the even components of the force ripple and the friction force can be separated easily from the even disturbances. If the identified force ripple and friction force have a lot of differences comparing with actual values, the tracking errors have some oscillation during the constant velocity motion and become very bigger at the start motion.

Fig. 8(b) shows the even parts of the friction force without the even components presented in (20). When these disturbances are rearranged in the position domain, the force ripple can be described as a function of the position. The identified force ripples are presented in Fig. 8(c), and the nominal force ripple determined by averaging of these results is noted as 'nom' from this figure. The even components of the friction force shown in Fig. 8(d) will be utilized to estimate the friction force model with the hysteresis effect.

The friction force is estimated by its odd disturbances and its even components. In the obtained odd disturbances, one half of the total samples have dominant characteristics of the friction force when the velocity is positive, while the remaining samples have dominant characteristics when the velocity is negative, as shown in Fig. 9(a). Therefore, the obtained odd disturbances can be separated according to the moving direction of the mover. These results of the even components of the friction force shown in Fig. 8(d) are presented simultaneously in Fig. 9(b). To identify the total friction force with the hysteresis effect, both components shown in Fig. 9(b) are combined and shown in Fig. 9(c). When the combined results are rearranged in the velocity domain, the data distribution for identifying the friction force model is obtained as shown in Fig. 9(d). Prior to identifying the dynamic friction force model, the parameters of the static friction force model are identified by (22). The identified parameters are presented in Table 3, and the static friction force model containing these parameters (noted as 'nom'; black dotted-line) is shown in Fig. 9(d). The identified static friction force model can be utilized for all the operating conditions of PMLSM-based motion systems by using the same parameters because it represents the friction force at the steady state. Moreover, the parametric variation is small.

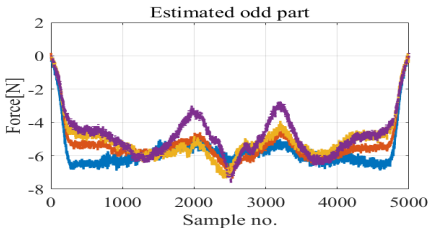

(a)

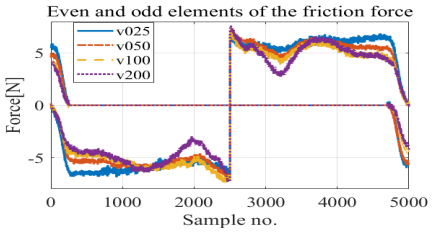

(b)

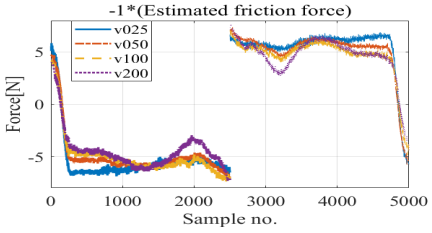

(c)

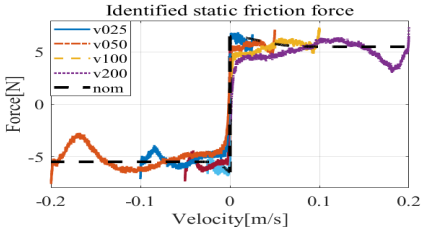

(d)

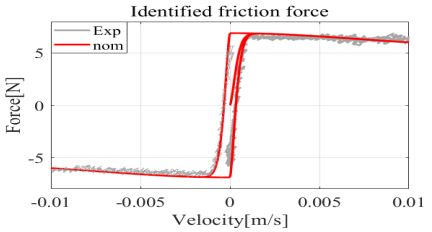

(e)

FIGURE 9. Identification of the friction force: (a) Odd parts in the sample domain. (b) Odd parts and even elements of the friction force separated along the moving direction in the sample domain. (c) Sum of even and odd elements of the friction force in the sample domain. (d) Identified static friction force in the velocity domain. (e) Identified friction force in the velocity domain (EXP1: v025).

On the other hand, the parameters of the dynamic friction force can be different since its dynamic characteristics such as the hysteresis effects vary according to many operating factors such as the rate of applied force and the dwell-time of the mover [28]. In this study, EXP1(v025) is utilized to identify the parameters of the dynamic friction force since the industrial applications of PMLSM-based motion systems requires the stop motion, which can be described by the dwell-time in EXP1 as it is long enough. Using (26), the parameters of the dynamic friction force model in (25) were identified as $\hat{\rho}_0 = 350500$ and $\hat{\rho}_1 = 1000$, and the identified dynamic friction force model is presented in Fig. 9(e). As shown here, it can be verified that the identified friction force model can describe the data distribution of the estimated hysteresis effect of the friction force very well. Of course, the hysteresis effects occurring by other reference trajectories can also be described by (26) and (27).

From these results, it is concluded that the proposed disturbance identification scheme can identify the parametric errors as well as the force ripple and the friction force with the hysteresis effects without using any conservative assumption and additional hardware setup such as sensors. Additionally, it is verified that the proposed scheme is quite simple and effective compared to other existing identification methods because only the even and odd characteristics of the disturbances are utilized.

TABLE 3. Identified parameters for the static friction force model.

Parameters	θ_1	θ_2	θ_3
values	6.5	5.5	0.010

TABLE 4. Control parameters of the compared controllers.

	Kp	Ki	Kd	M_n	B_n	Q-filter
value	263778	8839318	2543	8.7	80.7	33Hz

F. POSITION TRACKING PERFORMANCE

To verify the effectiveness of the identified parametric errors, force ripple, and friction force, the tracking performance is evaluated when the identified disturbances are utilized as a feedforward controller. This is done by comparing with the tracking performances of other controllers as follows:

- PID : A PID controller with only the feedforward controller of the inverse nominal model. (5) and (6) are utilized as control inputs. This controller is designed by only the nominal model.
- DOB : A PID controller with a linear disturbance observer. The control input is identical to (4) and requires no disturbance models to compensate for the disturbances.
- FF : A PID controller with the feedforward controller that consists of the identified disturbances. The control input consists of (5), (6), and $\Delta\hat{M}\ddot{x}_d(t) + \Delta\hat{B}\dot{x}_d(t) + \hat{F}_{rip}(x_d(t)) + \hat{F}_{fric}(\dot{x}_d(t))$. This controller is designed to evaluate the performance of direct compensation by the identified disturbances.

All control parameters are presented in Table. 4

The trapezoidal reference position trajectory is utilized to evaluate the validity of the identified force ripple. Since the reference velocity trajectory has a constant velocity region for 1.6sec and the effective stroke (40cm) is long enough, a force

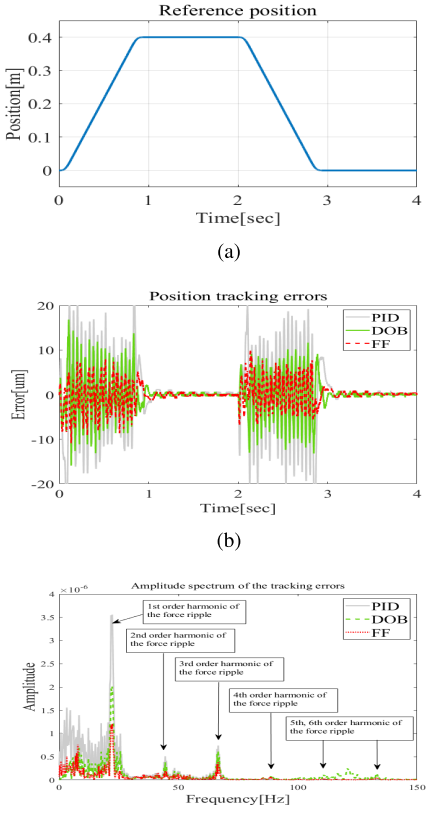

FIGURE 10. Reference trajectories in CASE1: (a) Reference position trajectory (maximum position: 0.400*m*). (b) Position tracking errors in comparative study. (c) Amplitude spectrum of (b) in comparative study.

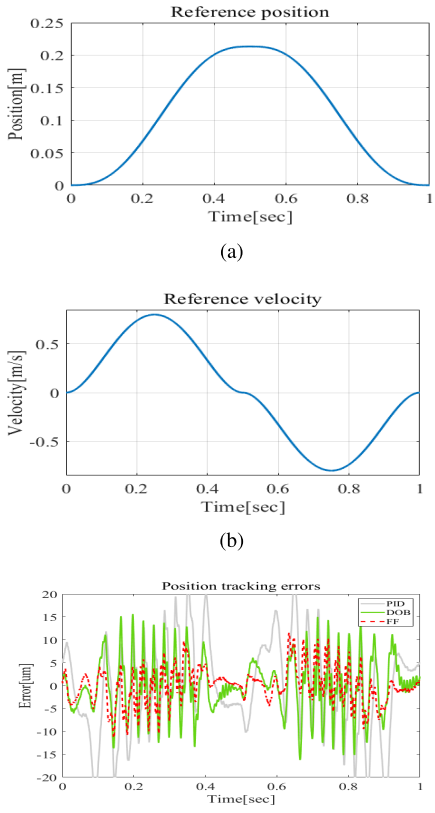

FIGURE 11. Reference trajectories in CASE2: (a) Reference position trajectory (maximum position: 0.213*m*). (b) Reference velocity trajectory. (c) Position tracking errors in comparative study.

TABLE 5. RMS and maximum position tracking errors in the trapezoidal reference trajectory.

	FF	PID	DOB
RMS[um]	2.63	7.49	3.97
MAX[um]	10.95	36.48	16.81

ripple occurs having an invariant fundamental frequency at various positions. Thus, it is appropriate to evaluate the effectiveness of the identified force ripple. The utilized reference trajectories are shown in Fig. 10(a). Here, the dominant fundamental frequency of the force ripple can be calculated as 22.22Hz since the maximum velocity is 0.5m/s. Since a stop motion exists, this trajectory is also appropriate to evaluate the validity of the identified friction force.

The tracking performance results of the comparative studies are shown in Fig. 10(b). The largest tracking errors occurred in the PID because it could not attenuate the force ripple and friction force. In the case of the DOB, the tracking performance was better than that of the PID, but the tracking errors when the mover of PMLSM-based motion system was moving were still larger than those of the FF. Since the Q-filter having a cutoff frequency of 33Hz is utilized due to the noise and unmodeled dynamics, the DOB cannot estimate and attenuate components of the force ripple over the fundamental frequency. On the other hand, the FF showed the best tracking performance among these controllers although the identified disturbances were obtained from the lumped disturbance estimated by the DOB. Especially, due to the identified force ripple, the tracking errors when the mover was moving were reduced. To verify the attenuation performance of the force ripple, the amplitude spectrum results of the tracking errors were obtained as presented in Fig. 10(c). From these results, it is verified that the FF, which uses the identified model information using the proposed scheme, can attenuate dominant frequency components of the force ripple more than the PID and DOB, even including components over the fundamental frequency of the force ripple.

To verify the robustness of the proposed scheme, the bell-type reference position trajectory has been also utilized as shown in Fig. 11(a). Comparing to the trapezoidal position trajectory, there is no stop motion in this trajectory as shown in Fig. 11(b). Since the moving direction changes faster than the trapezoidal position trajectory, the disturbances are also varied depending on the position and velocity. Therefore, it is appropriate to evaluate the robustness of the proposed control scheme using identified parameters. As shown in Fig. 11(c), DOB showed better tracking performance than the PID. But, it existed the limitation of the improvement of the tracking performance due to the bandwidth of Q-filter in DOB. On the other hand, the FF showed the best tracking

TABLE 6. RMS and maximum position tracking errors in the bell-type reference trajectory.

	FF	PID	DOB
RMS[um]	3.98	5.88	10.04
MAX[um]	11.68	16.24	25.83

performance since the distortion of the phase and magnitude of the disturbance estimated by DOB and the characteristics of the friction force induced at the fast reversal motion were compensated by the proposed identification scheme. Therefore, we can conclude that the robustness of proposed control scheme using the identified parameters are guaranteed.

V. CONCLUSION

Many system identification methods are used to identify the key parameters in PMLSM-based motion systems. Using sine sweep input signals showed that the linear parameters of PMLSM-based motion systems can be obtained easily by frequency responses of the transfer function. However, nonlinear disturbances such as the friction force and the force ripple are not identified easily due to the coupled characteristics of these disturbances. To address this problem, a disturbance identification method was presented. In the proposed scheme, the disturbances such as the parametric errors, force ripple, and friction force were identified and separated from a lumped disturbance by using even and odd characteristics of the state-dependent disturbances. Comparing with existing disturbance methods, this proposed scheme proved to be a very simple and powerful identification method, and it required no conservative assumptions and additional hardware setups. Through various experimental tests, it was verified that the identified disturbances could improve the tracking performance directly. However, the proposed scheme is found to have limitation of the estimated disturbances due to the cutoff frequency of Q-filter in DOB. In the future, the frequency range of the estimated lumped disturbance must be improved by advanced disturbance observers. Also, the convergence analysis of estimated disturbances should be supplemented by theoretical proofs although the boundness of the estimated disturbances is shown by experimental results.

REFERENCES

[1] M. Iwasaki, K. Seki, and Y. Maeda, "High-precision motion control techniques: A promising approach to improving motion performance," *IEEE Ind. Electron. Mag.*, vol. 6, no. 1, pp. 32–40, Mar. 2012.
[2] K. Saiki, A. Hara, K. Sakata, and H. Fujimoto, "A study on high-speed and high-precision tracking control of large-scale stage using perfect tracking control method based on multirate feedforward control," *IEEE Trans. Ind. Electron.*, vol. 57, no. 4, pp. 1393–1400, Apr. 2010.
[3] T. Yamaguchi, M. Hirata, and J. Pang, *High-Speed Precision Motion Control*. Boca Raton, FL, USA: CRC Press, 2011.
[4] A. Amthor, S. Zschaeck, and C. Ament, "High precision position control using an adaptive friction compensation approach," *IEEE Trans. Autom. Control*, vol. 55, no. 1, pp. 274–278, Jan. 2010.
[5] L. Lu, Z. Chen, B. Yao, and Q. Wang, "Desired compensation adaptive robust control of a linear-motor-driven precision industrial gantry with improved cogging force compensation," *IEEE/ASME Trans. Mechatronics*, vol. 13, no. 6, pp. 617–624, Dec. 2008.
[6] R. Cao and K.-S. Low, "A repetitive model predictive control approach for precision tracking of a linear motion system," *IEEE Trans. Ind. Electron.*, vol. 56, no. 6, pp. 1955–1962, Jun. 2009.
[7] J.-S. Chen, K.-C. Chen, Z.-C. Lai, and Y.-K. Huang, "Friction characterization and compensation of a linear-motor rolling-guide stage," *Int. J. Mach. Tools Manuf.*, vol. 43, no. 9, pp. 905–915, Jul. 2003.
[8] L. Bascetta, P. Rocco, and G. Magnani, "Force ripple compensation in linear motors based on closed-loop position-dependent identification," *IEEE/ASME Trans. Mechatronics*, vol. 15, no. 3, pp. 349–359, Jun. 2010.
[9] G. Ferretti, G. Magnani, and P. Rocco, "Modeling, identification, and compensation of pulsating torque in permanent magnet AC motors," *IEEE Trans. Ind. Electron.*, vol. 45, no. 6, pp. 912–920, 1998.
[10] C. Rohrig and A. Jochheim, "Identification and compensation of force ripple in linear permanent magnet motors," in *Proc. Amer. Control Conf.*, vol. 3, Jun. 2001, pp. 2161–2166.
[11] P. Van Den Braembussche, J. Swevers, H. Van Brussel, and P. Vanherck, "Accurate tracking control of linear synchronous motor machine tool axes," *Mechatronics*, vol. 6, no. 5, pp. 507–521, Aug. 1996.
[12] Z. Jamaludin, H. Van Brussel, and J. Swevers, "Quadrant glitch compensation using friction model-based feedforward and an inverse-model-based disturbance observer," in *Proc. 10th IEEE Int. Workshop Adv. Motion Control*, Mar. 2008, pp. 212–217.
[13] H. Asaumi and H. Fujimoto, "Proposal on nonlinear friction compensation based on variable natural length spring model," in *Proc. SICE Annu. Conf.*, Aug. 2008, pp. 2393–2398.
[14] Y. Maeda and M. Iwasaki, "Analytical examinations and compensation based on rolling friction model for slow settling response in precise positioning," *IEEJ Trans. Ind. Appl.*, vol. 129, no. 12, pp. 1218–1225, 2009.
[15] T. Takemura and H. Fujimoto, "Proposal of novel rolling friction compensation with data-based friction model for ball screw driven stage," in *Proc. 36th Annu. Conf. IEEE Ind. Electron. Soc. (IECON)*, Nov. 2010, pp. 1932–1937.
[16] K. K. Tan, T. H. Lee, H. Dou, and S. Zhao, "Force ripple suppression in iron-core permanent magnet linear motors using an adaptive dither," *J. Franklin Inst.*, vol. 341, no. 4, pp. 375–390, Jul. 2004.
[17] S. Zhao and K. K. Tan, "Adaptive feedforward compensation of force ripples in linear motors," *Control Eng. Pract.*, vol. 13, no. 9, pp. 1081–1092, Sep. 2005.
[18] J. Yao, Z. Jiao, and D. Ma, "Adaptive robust control of DC motors with extended state observer," *IEEE Trans. Ind. Electron.*, vol. 61, no. 7, pp. 3630–3637, Jul. 2014.
[19] H. Pan, W. Sun, H. Gao, and X. Jing, "Disturbance observer-based adaptive tracking control with actuator saturation and its application," *IEEE Trans. Autom. Sci. Eng.*, vol. 13, no. 2, pp. 868–875, Apr. 2016.
[20] H. Pan and W. Sun, "Nonlinear output feedback finite-time control for vehicle active suspension systems," *IEEE Trans. Ind. Informat.*, vol. 15, no. 4, pp. 2073–2082, Apr. 2019.
[21] H. Pan, X. Jing, W. Sun, and H. Gao, "A bioinspired dynamics-based adaptive tracking control for nonlinear suspension systems," *IEEE Trans. Control Syst. Technol.*, vol. 26, no. 3, pp. 903–914, May 2018.
[22] K. Cho, J. Kim, S. B. Choi, and S. Oh, "A high-precision motion control based on a periodic adaptive disturbance observer in a PMLSM," *IEEE/ASME Trans. Mechatronics*, vol. 20, no. 5, pp. 2158–2171, Oct. 2015.
[23] W. Deng and J. Yao, "Extended-State-Observer-Based adaptive control of electrohydraulic servomechanisms without velocity measurement," *IEEE/ASME Trans. Mechatronics*, vol. 25, no. 3, pp. 1151–1161, Jun. 2020.
[24] W. Deng, J. Yao, and D. Ma, "Time-varying input delay compensation for nonlinear systems with additive disturbance: An output feedback approach," *Int. J. Robust Nonlinear Control*, vol. 28, no. 1, pp. 31–52, Jan. 2018.
[25] T. Umeno and Y. Hori, "Robust speed control of DC servomotors using modern two degrees-of-freedom controller design," *IEEE Trans. Ind. Electron.*, vol. 38, no. 5, pp. 363–368, Oct. 1991.
[26] M. Tomizuka, "Model based prediction, preview and robust controls in motion control systems," in *Proc. 4th IEEE Int. Workshop Adv. Motion Control (AMC-MIE)*, vol. 1, 1996, pp. 1–6.
[27] C. C. de Wit, H. Olsson, K. J. Åström, and P. Lischinsky, "A new model for control of systems with friction," *IEEE Trans. Autom. Control*, vol. 40, no. 3, pp. 419–425, Mar. 1995.
[28] J. Wojewoda, A. Stefański, M. Wiercigroch, and T. Kapitaniak, "Hysteretic effects of dry friction: Modelling and experimental studies," *Phil. Trans. Roy. Soc. A, Math., Phys. Eng. Sci.*, vol. 366, no. 1866, pp. 747–765, Mar. 2008.

KWANGHYUN CHO (Member, IEEE) received the B.S. degree in electrical engineering and computer science from Kyungpook National University, Daegu, South Korea, in 2008, and the M.S. and Ph.D. degrees in mechanical engineering from the Korea Advanced Institute of Science and Technology (KAIST), Daejeon, South Korea, in 2010 and 2014, respectively. He is currently a Senior Engineer with the Mechatronics Research and Development Center, Samsung Electronics Company Ltd., Hwaseong, Korea. His research interest includes precision motion control based on linear motors.

KANGHYUN NAM (Member, IEEE) received the B.S. degree in mechanical engineering from Kyungpook National University, Daegu, South Korea, in 2007, the M.S. degree in mechanical engineering from the Korea Advanced Institute of Science and Technology, Daejeon, South Korea, in 2009, and the Ph.D. degree in electrical engineering from The University of Tokyo, Tokyo, Japan, in 2012.

From 2012 to 2015, he was a Senior Engineer with Samsung Electronics Company Ltd., South Korea. Since 2015, he has been an Assistant Professor with the School of Mechanical Engineering, Yeungnam University, South Korea. His research interests include motion control, vehicle dynamics and control, and electric vehicles. He is also a member of the Korean Society of Automotive Engineers. He received the 2013 Best Paper Award from the IEEE TRANSACTION ON INDUSTRIAL ELECTRONICS in 2014.